Electron-paramagnetic-resonance study of Cu^{2+}- and Mn^{2+}-doped $LiCsSO_4$ single crystals: $LiCsSO_4$ phase transitions

Sushil K. Misra and Lucjan E. Misiak*
Physics Department, Concordia University, 1455 de Maisonneuve Boulevard West, Montreal, Quebec, Canada H3G 1M8
(Received 26 April 1993)

EPR studies on Mn^{2+}-doped $LiCsSO_4$ single crystals were performed in the temperature range 3.8–301 K, as well as on Cu^{2+}-doped $LiCsSO_4$ single crystals at room temperature. At higher temperatures the crystals were found to consist of twin domains. There were detected two phase transitions, one of which occurs at 205 K, and the other one is spread over the temperature range 155–175 K. In addition, the occurrence of a third phase transition somewhere in the range 3.8–31 K has been confirmed by the present data. The values of the isotropic g factor and the hyperfine-interaction constant for Mn^{2+} have been estimated at room temperature. Further, the values of all the Mn^{2+} spin-Hamiltonian parameters g, b_2^0, b_2^2, b_4^0, b_4^2, b_4^4, Q', Q'', $A_\parallel$, $A_\perp$ have been estimated at 90 and 152 K in the untwinned monoclinic phase. The intensity of the central broad Mn^{2+} line (hyperfine structure unresolved) is described well as a function of temperature, near T_c, by the expression $c|T-T_c|^\gamma+b$ ($T_c=205$ K), with the critical exponent $\gamma=1$, in accordance with that determined previously for the elastic constant c_{66}.

I. INTRODUCTION

Lithium cesium sulfate ($LiCsSO_4$) (LCS hereafter) crystals have been studied by optical and Raman spectroscopy,[1–4] electron-paramagnetic-resonance (EPR) of the NH_3^+ ion (stabilized by the CrO_4^{-2} ion) and that of the SO_3^- ion (produced by γ- or x-ray irradiation),[5–9] ultrasonic technique,[10] Brillouin spectroscopy,[11,12] NMR of ^7Li and ^{133}Cs nuclei,[13,14] x-ray diffraction,[15–17] thermal expansion,[18] differential scanning calorimetry,[19] and specific-heat measurements.[20]

As the temperature is lowered from room temperature (RT), LCS crystals undergo a transition from the paraelastic phase with orthorhombic structure (*Pcmn* space group; *mmm* point group) to the ferroelastic phase with monoclinic structure ($P2_1/n$ space group; $2/m$ point group) without undergoing a change in the number of atoms in the unit cell at about 202 K,[2,9,11,19] as determined by the x-ray technique.[15–17] Kruglik *et al.*[15] reported a microscope observation of an intermediate phase in LCS between 199–206 K. The EPR of the NH_3^+ radical indicated the occurrence of a phase transition in LCS at 206 K;[5,8] determined to be of second order by Pietraszko, Tomaszewski, and Łukaszewicz[17] by x-ray diffraction, and further confirmed by the observation of an anomaly of the specific heat (without latent heat) in calorimetric measurements[20] at the transition temperature. The value of the elastic constant (c_{66}) of LCS has been observed to decrease with lowering temperature, above T_c, indicating softening.[10,11] More recently, Raman scattering [2] indicated the occurrence with lowering temperature in LCS of (i) a structural phase transition at 202 K, (ii) an incommensurate-commensurate phase transition at about 160 K, and (iii) a structural phase transition of the unlocking type below 20 K as deduced from the observation of soft phonons in the temperature range just above 20 K.

LCS crystals are interesting because they exhibit unexpected features. For example, in LCS the volume thermal-expansion coefficient (β) decreases with warming across the phase transition (203 K) from the orthorhombic to the monoclinic phase,[20] while usually it increases on warming, and the phase-transition temperature in LCS has been observed to decrease with decreasing pressure,[21] contrary to that observed in some other crystals of this family, e.g., $LiNH_4SO_4$ (Ref. 22) and $LiKSO_4$ (Ref. 23).

In order to further study the phase transitions undergone by LCS, Mn^{2+} ions were incorporated in $LiCsSO_4$ crystals to serve as paramagnetic probes in the present detailed EPR temperature variation study, carried out in the temperature range 3.8–301 K. It is difficult to grow single crystals of LCS with sufficient doping of transition-metal ions (see Sec. II). Perhaps for this reason no EPR study has so far been reported on LCS crystals doped with Mn^{2+} and Cu^{2+} ions. It is expected that the temperature dependence of the EPR spectra, as well as those of the linewidth and the intensity of the EPR lines, would provide detailed information on the nature of the phase transitions in LCS. In addition, Cu^{2+} EPR data were recorded on Cu^{2+}-doped LCS crystals to better understand the room temperature (RT) behavior of these crystals.

Details on the preparation of samples and the experimental arrangement are described in Secs. II and III, respectively. The EPR spectra, and their interpretation by comparison with similar systems are discussed in Secs. IV and V, respectively. The evaluation of the spin-Hamiltonian parameters, and the critical exponent (γ) are presented in Secs. VI and VII, respectively. The details of the occurrences of phase transitions in LCS crystals are given in Sec. VIII. The concluding remarks are made in Sec. IX.

II. SAMPLE PREPARATION AND CRYSTAL STRUCTURE

$LiCsSO_4$ single crystals doped with 0.5, 1.0, 1.5, and 5.0 mol. % of $MnSO_4$ and $CuSO_4$ were grown at room temperature from aqueous solutions containing equimolar proportions of Li_2SO_4 and Cs_2SO_4. The as-grown crystals were clear and colorless. Only a few crystals exhibited well-resolved hyperfine lines in the EPR spectrum of Mn^{2+}. The EPR spectra revealed that the numbers of Mn^{2+} and Cu^{2+} ions entering LCS crystals were rather small, being independent of the initial concentrations of these ions in the respective solutions.

Mn^{2+} ions can either substitute for Li^+ or Cs^+ ions in LCS, or they can occupy an interstitial site. In any case, a cation vacancy is created subsequent to incorporation to compensate for the overall charge. This vacancy can become bound to the Mn^{2+} ion forming a pair. On the other hand, in place of substitution or interstitial incorporation, Mn^{2+} ions may form ion clusters.

The growth habit of as-grown LCS crystals is shown in Fig. 1(a). It is usually in the form of a pseudohexagonal plate composed of six 60° twin domains, the c axis for any twin domain being perpendicular to the hexagonal plate, while its b axis being parallel to the outer edge. (The twin domains disappear below 160 K, as revealed by the EPR of NH_3^+ and Cr^{5+} ions in LCS by Yu, Chou, and Huang.[5]) Figure 1(b) depicts the projections of atoms from one layer of $LiCsSO_4$ tetrahedra in the orthorhombic ($T > T_c$; $T_c \simeq 205$ K) and monoclinic ($T < T_c$) phases. The crystal structure of LCS (Ref. 15) in the paraelastic phase, above the phase-transition temperature (T_c) is orthorhombic (D_{2h}^{16}-*Pcmn* space group) with the unit-cell parameters $a = 0.9456(2)$, $b = 0.5456(1)$, $c = 0.8820(3)$ nm, $z = 4$, whereas in the ferroelastic phase ($T < T_c$) it is monoclinic (C_{2h}^5-$P2_1/n$ space group) with the unit-cell parameters $a = 0.9379(2)$, $b = 0.5423(1)$, $c = 0.8834(3)$ nm, $\gamma = 89.75°$, and $z = 4$ [Fig. 1(b)].

The four Cs atoms, as well as the four SO_4 groups are crystallographically equivalent in the unit cell of LCS.

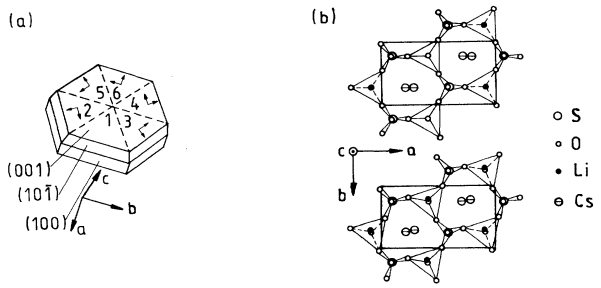

FIG. 1. (a) The room-temperature crystal growth habit of $LiCsSO_4$ single crystals, composed of six twin domains. The orientations of the crystal a, b axes for domain 1 are indicated below the figure, while those for domains 2–6 are indicated by small arrows in the domains themselves. (b) Projections of atoms from one layer of $LiCsSO_4$ tetrahedra in the orthorhombic phase (*Pcmn* symmetry—upper plot, $T > T_c = 205$ K) and in the monoclinic phase ($P2_1/n$ symmetry—lower plot, $T < T_c$) onto the ab crystal plane.

The oxygen coordination around each Cs atom is 11-fold and the Cs-O distances are in the range 0.3235–0.3633 nm (average distance = 0.3388 nm).[15]

III. EXPERIMENTAL ARRANGEMENT

A Varian V4502 X-band spectrometer equipped with a 12-inch electromagnet, along with a Bruker power supply (type B-MN50/200) and a Bruker field controller (B-H15), was employed for EPR measurements. A cryostat with a medium-Q cavity, capable of temperature control, was used for liquid-helium temperature measurements. As well, some measurements were made using a high-Q cavity nitrogen gas flow Varian temperature controller (E4540) with a temperature stability of better than 0.5 K (between RT and 125 K). The samples were oriented inside the microwave cavity after inspection under a microscope in such a way that the external magnetic-field direction could be varied in chosen crystal planes.

IV. EPR SPECTRA

The EPR spectra of Mn^{2+}-doped LCS crystals were recorded in the temperature range 3.8–301 K. On the other hand, the EPR measurements on Cu^{2+}-doped LCS crystals were confined to room temperature, because detailed information about the crystalline environment indicating the phase transition cannot be obtained from Cu^{2+} spectra. The electronic spin of this ion is $S = \frac{1}{2}$, thus its spin Hamiltonian does not contain terms reflecting the crystalline electric field.

Cu^{2+}

The RT Cu^{2+} spectra as recorded for **B**||**a**, **b**, and 45° from the a axis in the ab plane for LCS sample I, and for **B**||**a**, **b** for LCS sample II, are exhibited in Fig. 2. For each orientation, the Cu^{2+} ions exhibit a three-lines overlapping spectrum; the three lines correspond to three magnetically inequivalent Cu^{2+} centers belonging to different twin domains. The hyperfine structure of any line is unresolved. (When resolved, each Cu^{2+} center has four EPR hyperfine lines, corresponding to the electronic spin-$\frac{1}{2}$, and the nuclear spin-$\frac{3}{2}$ of each of the two isotopes whose nuclear magnetic moments are approximately equal to each other in value.) The positions of these three lines were observed to be sensitive to the orientation of **B**.

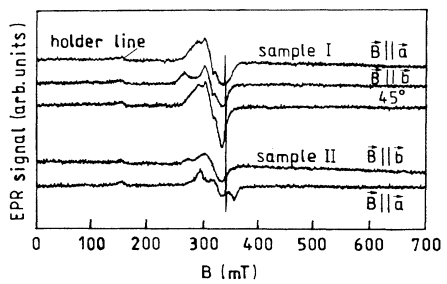

FIG. 2. EPR spectra of Cu^{2+}-doped $LiCsSO_4$ crystals (samples I and II) for different orientations of the external magnetic field in the ab plane at 297 K.

The estimated g values as evaluated from the line positions corresponding to the three Cu^{2+} centers for sample I are 2.564, 2.177, 2.035 (for **B**||**b**) and 2.342, 2.186, 2.022 (for **B**||**a**). These values are close to the principal values of the g tensor estimated for Cu^{2+}-doped $LiKSO_4$ characterized by a rhombic local symmetry.[24] The EPR spectra of sample II consist of two (**B**||**b**) and three (**B**||**a**) lines, corresponding to three Cu^{2+} centers belonging to different twin domains; in the former case there is overlapping of lines due to Cu^{2+} ions belonging to different domains. The corresponding g values are 2.508, 2.141, 2.141 (for **B**||**b**) and 2.318, 2.094, 1.917 (for **B**||**a**). The difference in the Cu^{2+} g values in samples I and II may be due to different structures of the domains.

Mn^{2+}

In general, the EPR spectrum of a Mn^{2+} center consists of five sextets corresponding to the electronic spin $S=\frac{5}{2}$ and nuclear spin $I=\frac{5}{2}$. Each sextet corresponds to the allowed transitions $M,m \leftrightarrow (M-1),m$ where M $(=\pm\frac{5}{2},\pm\frac{3}{2},\pm\frac{1}{2})$ is the electronic magnetic quantum number and m $(=\pm\frac{5}{2},\pm\frac{3}{2},\pm\frac{1}{2})$ is the nuclear magnetic quantum number. Figure 3 shows Mn^{2+} EPR spectra in LCS for **B**||**c** at RT, and for **B**||**b** at several temperatures from RT down to 3.8 K. (Here **b**, **c** are vectors along the b,c axes of the crystal, respectively.) The RT Mn^{2+} spectrum exhibits for **B**||**b**,**c** among other (hyperfine) lines of very weak intensity, a set of six hyperfine (hf) lines, referred to hereafter as the central sextet (A) centered at $\sim$325 mT. In addition, the RT spectrum for **B**||**b** exhibits another intense broad line (B), located at $\sim$220 mT, whose hf structure is not resolved. (In the following discussion, only the intense EPR lines will be considered, unless otherwise stated.)

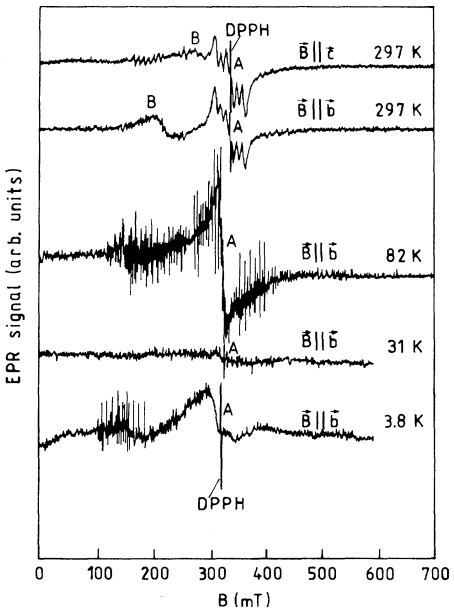

FIG. 3. EPR spectra at 3.8, 31, 82, and 297 K of a Mn^{2+}-doped $LiCsSO_4$ crystal for the orientation of the external magnetic field (**B**) parallel to the b axis (**B**||**b**), as well as that for **B**||**c**, at 297 K.

Figure 4 shows the angular variation of the line positions of all the observed lines, weak or intense, for the rotation of **B** in the *ab* and *ac* planes at RT. The position of the broad line B is found to vary significantly with the orientation of the magnetic field (**B**). Further, it is seen from Fig. 4 that at RT the positions of the hf lines corresponding to the central sextet (A) are isotropic, i.e., independent of the orientation of the external magnetic field (**B**).

It is noted that in Figs. 3 and 4 the central sextet (A) and the broad line (B) may belong the different Mn^{2+} centers, located perhaps in different twin domains.

It is seen from Fig. 5, displaying the Mn^{2+} EPR spectra for **B** at $-25°$ from the c axis in the *ac* plane at selected temperatures between 125 and 301 K, that the intensities of the Mn^{2+} hf lines other than those belonging to the central sextet (A), increase significantly at lower temperatures as compared to those at RT. This is particularly true of the highest-field sextet, whose position moves somewhat towards lower fields as the temperature is decreased, and which is observed at all temperatures between 125 and 301 K. On the other hand, the intensity of the hf lines of the central sextet (A) gradually decreases with lowering temperature. Finally, the hf splitting of the central sextet vanishes completely at 248 K, there appearing only a broad line (referred to as the broad line A, hereafter, for $T<248$ K). Below 248 K, there still appear the broad lines A and B, as well some overlapping hf lines corresponding to the Mn^{2+} centers belonging to different twin domains. As the temperature was lowered further to 160 K (the spectrum is not shown in Fig. 5 at this temperature), there emerged a third broad line (C) (indicted in the spectrum at 138 K in Fig. 5), without hyperfine splitting, centered at $\sim$74 mT. The emergence of this new line indicated the occurrence of a phase transition. (For more details, see Sec. VIII.)

Figure 6 displays the angular variation of all the Mn^{2+} line positions, weak or intense, in LCS: (a) at 248 K for the orientation of **B** in the *ac* plane and (b) at 3.8 K for the orientation of **B** in the *ab* plane. From these figures, it is seen that the central broad line A is isotropic with respect to the orientation of **B** in the *ac* and *ab* planes, and is both observed at 248 and 3.8 K. Further, line B, observed at 248 K, disappears at 3.8 K.

Figure 7 shows the first derivative peak-to-peak linewidth (ΔB_{pp}) of the four outer hyperfine resonance transition lines of the central sextet (belonging to $m=\pm\frac{5}{2},\pm\frac{3}{2}$) as functions of temperature for **B** at $-25°$ from the c axis in the *ac* plane between 252–301 K. (The hf lines for $m=\pm\frac{3}{2}$ are not resolved below 271 K.) In general, there is observed a broadening of these four lines with the lowering of temperature. The outermost hf lines ($m=\pm\frac{5}{2}$) broaden much more than the adjacent ones ($m=\pm\frac{3}{2}$).

In Fig. 8 are plotted the peak-to-peak heights of the first-derivative line shape (I) of the broad lines A for the orientation of **B** at $+10°$ from the a axis in the *ab* plane and for **B** at $-25°$ from the c axis in the *ac* plane (I for

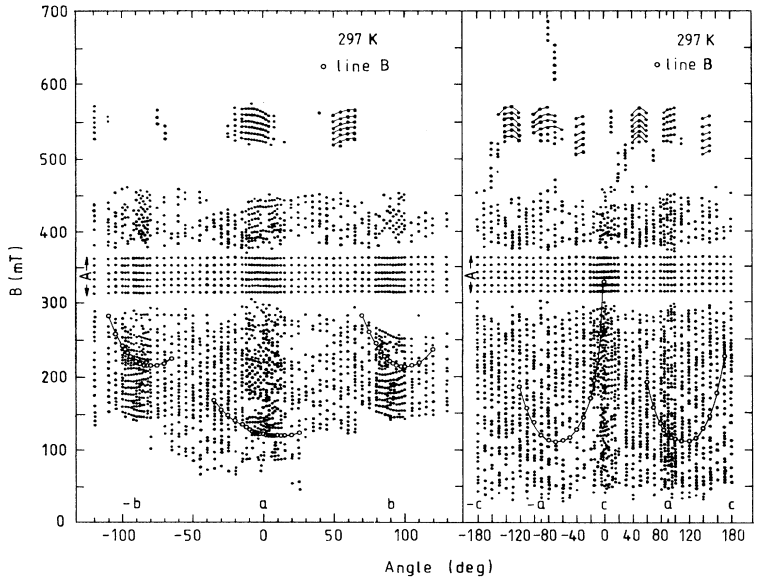

FIG. 4. Angular variation of the EPR line positions for a Mn^{2+}-doped $LiCsSO_4$ crystal at 297 K for the orientation of the external magnetic field in the *ab* and *ac* planes. The data points indicated by "○" indicate the broad line *B*. It should be noted that there are more lines indicated here than those clearly visible in the spectra exhibited in Fig. 3 at 297 K. This is because these spectra have been reduced considerably, so that many of the lines with relatively low intensity are not clearly seen.

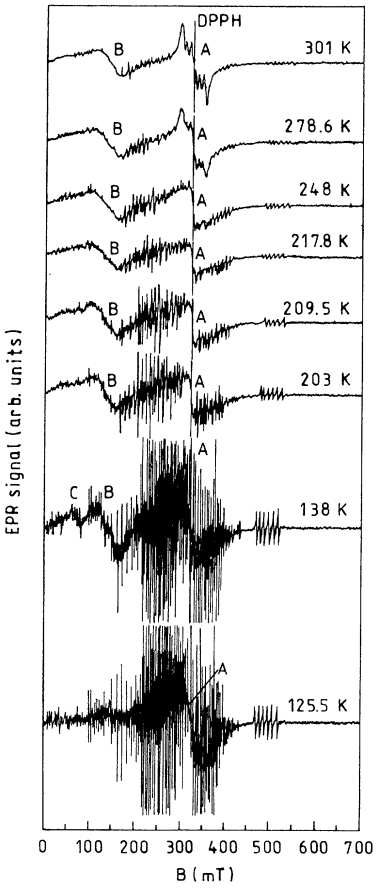

FIG. 5. EPR spectra of Mn^{2+}-doped $LiCsSO_4$ crystal in the temperature range 125–301 K for the orientation of the external magnetic field at −25° from the *c* axis in the *ac* plane.

line *B* is not plotted for **B** at +10° from the *a* axis in the *ab* plane, because of low intensity at this orientation), as well as the peak-to-peak height (I) of the broad line *B* for **B** at −25° from the *c* axis in the *ac* plane and the peak-to-peak width (ΔB_{pp}) of the line *B* for **B** at −25° from the *c* axis in the *ac* plane as functions of temperature in the range 125–301 K. (Above 248 K, it is the overall the peak-to-peak height of the central sextet *A* ignoring the hyperfine structure, that is plotted. The peak-to-peak linewidth of line *A* is invariant with temperature, so it is not plotted.) The decrease of the height of line *A* as the temperature is lowered from RT to slightly above the phase-transition temperature T_c (=205 K), for the two orientations of **B** is in accordance with the reported decrease of value of the elastic constant c_{66} (corresponding to the spontaneous strain e_6, an order parameter) for the LCS crystal.[10,11] (For more details, see Sec. VII.)

Figure 9 exhibits full 30-line Mn^{2+} spectra for LCS at 90 and 152 K for **B** along a magnetic axis (lying close to the *c* axis in the *ac* plane), since for this orientation of **B** the Mn^{2+} hf lines due to two different Mn^{2+} centers become coincident. This axis is determined to be a magnetic axis after comparing with the angular variation of line positions at 248 K [Fig. 6(a)], and identified as the magnetic *x* axis after a study of the values of the spin-Hamiltonian parameters. (For more details see Sec. VI.)

V. INTERPRETATION OF LCS EPR SPECTRA BY COMPARISON WITH SIMILAR SYSTEMS

In order to interpret the Mn^{2+} spectra in LCS, specifically the presence at RT of the central sextet (or the central broad line *A* below 248 K), which may be due to the presence of Mn^{2+} clusters,[25] and the other broad lines *B* and *C*, assumed to be due to different Mn^{2+}

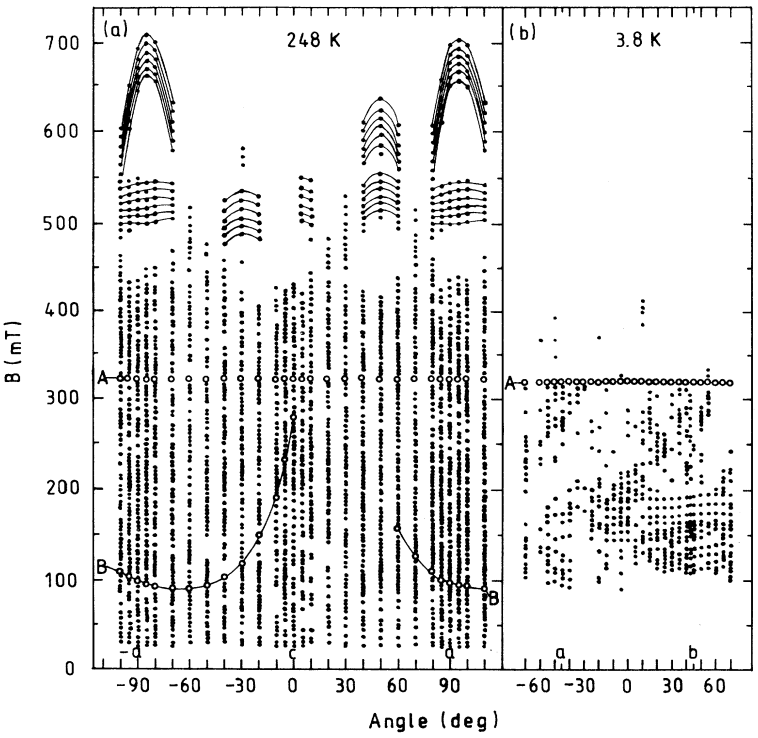

FIG. 6. Angular variation of the EPR line positions of Mn^{2+} in a $LiCsSO_4$ crystal: (a) at 248 K for the orientation of the external magnetic field (**B**) in the *ac* plane and (b) at 3.8 K for the orientation of **B** in the *ab* plane. The data points indicated by "○" characterize the broad lines *A* and *B*. It should be noted that there are more lines indicated here than those clearly visible in the spectra exhibited in Fig. 3 at 3.8 K and Fig. 5 at 248 K. This is because these spectra have been reduced considerably, so that many of the lines with relatively low intensity are not clearly seen.

centers, a comparison with those crystals where similar Mn^{2+} spectra were observed is now made.

p-GaAs

In this crystal there are observed, for $\mathbf{B}\|\langle 110\rangle$ at 8 K,[26] two broad Mn^{2+} lines in addition to the central sextet at magnetic-field values smaller than that of the central sextet. The two broad lines are interpreted to arise from a neutral manganese center (A^0:$\Delta M=1$, $\Delta M=2$) with the ground state ($3d^5$+hole). On the other hand, the hyperfine pattern of the central sextet ($g\approx 2$) is due to compensated manganese (A^-:$\Delta M=1$).

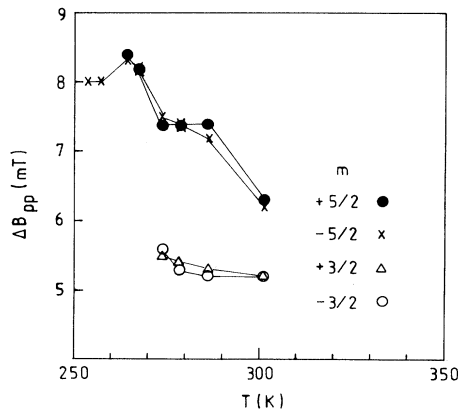

FIG. 7. First-derive peak-to-peak linewidths (ΔB_{pp}) of the individual hf lines of the central Mn^{2+} hyperfine sextet as functions of temperature in the range 246–301 K for the orientation of **B** at −25° from the *c* axis in the *ac* plane.

NH_4Br

Observation of only the Mn^{2+} central sextet ($g\approx 2$) at RT is also found in this crystal by Chand and Upreti.[25] The usual five sextets (30 lines) for Mn^{2+} were, indeed, observed in NH_4Br at liquid-nitrogen temperature as reported in the unpublished work of Sastry,[27] similar to the present data in LCS below 152 K (Fig. 9). However, Chand and Upreti[25] considered Sastry's observation to be wrong, because of lack of similar data in their EPR measurements on NH_4 Br.

$(TaSe_4)_2I$

Only the central isotropic Mn^{2+} sextet ($g\approx 2$), was observed in this crystal at temperatures above 250 K by Shaltiel *et al.*[28] They assumed that this was due either to the presence of strains in the sample which completely broaden out all the noncentral sextets, or due to the overall fine-structure splitting of Mn^{2+} being less than the hyperfine splitting of the central sextet. The latter situation is, however, not compatible with LCS, because for LCS there are observed other sextets in addition to the central one at RT (Fig. 3). According to Shaltiel *et al.*,[28] the quadrupole interactions between the charge-density waves and Mn^{2+} ions are responsible for the broadening of hf lines of the central sextet in Mn^{2+}-doped $(TaSe_4)_2I$ in the range 120–300 K.

RuS_2 and $RuSe_2$

Mn^{2+}-doped RuS_2 and $RuSe_2$ exhibit only the central sextet ($g\approx 2$),[29] interpreted to be exchange-narrowed (Lorentzian line shape), but dipolar-broadened

(temperature-dependent), lines of Mn^{2+}.

From the above one may conclude that the broad lines B and C which are observed in LCS in different temperature regions are possibly due to neutral manganese-vacancy centers. They are not due to different twin domains because line C occurs only below 162 K where the twinning is absent. On the other hand, the formation of either Mn^{2+} clusters, or the presence of strains,[28,30] or the binding of a vacancy with the Mn^{2+} ion,[25] may be responsible for the occurrence of the central Mn^{2+} sextet. Further, the broadening of its hf lines may be due to quadrupole interactions between the Mn^{2+} ion and charge-density waves.[28]

VI. EVALUATION OF Mn^{2+} SPIN-HAMILTONIAN PARAMETERS

Room temperature

At RT, only the Mn^{2+} central sextet, rather than a full 30-line (five sextets) spectrum, appears. Thus, only the values of the isotropic g_0 factor and the hyperfine parameter A_0 can be estimated by fitting the line positions

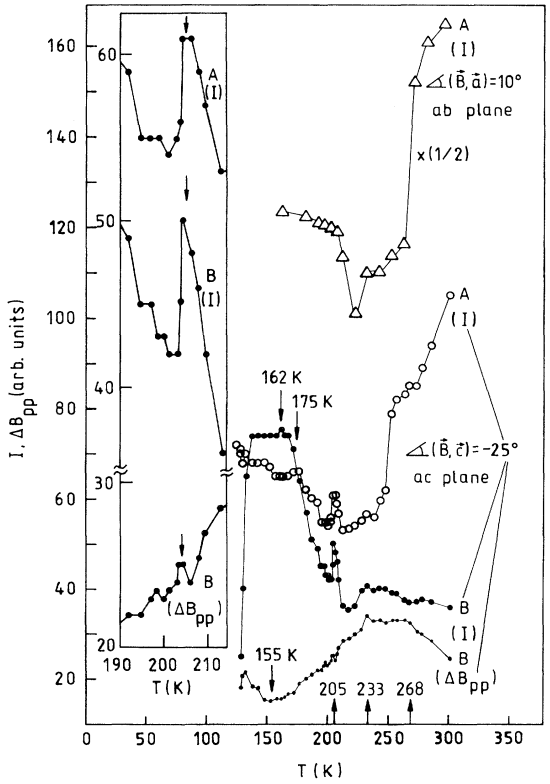

FIG. 8. The plots as functions of temperature in the range 125–301 K of the peak-to-peak height (I) of the broad line A for the orientation of **B** at $+10°$ from the a axis in the ab plane (△) and for **B** at $-25°$ from the c axis in the ac plane (○), as well as the height (I) of the broad line B (●) and the peak-to-peak width (ΔB_{pp}) of the broad line B (·) for **B** at $-25°$ from the c axis in the ac plane. The inset amplifies the plots of I for lines A and B and the width of line B for **B** at $-25°$ from the c axis in the ac plane in the temperature range 190–214 K.

($M=\frac{1}{2}, m \leftrightarrow M=-\frac{1}{2}, m$) of the isotropic central sextet A to the theoretical expression[25,31]

$$B_m = B_0 - A_0 m - \frac{A_0^2}{8B_0}(35-4m^2)$$

$$= \frac{g_D B_D}{g_0} - A_0 m - \frac{A_0^2 g_0}{8 g_D B_D}(35-4m^2)\,, \qquad (1)$$

where $B_0 = h\nu/g_0\mu_B$, and m, ν, h, g_D (=2.0036), and B_D are, respectively, the nuclear magnetic quantum number, the frequency of the klystron, Planck's constant, the g factor and the resonance line position for the free radical diphenyl-picryl-hydrazyl (DPPH).

The fitting yielded the values of $A_0 = -0.263 \pm 0.005$ GHz and $g_0 = 2.0054 \pm 0.0008$ for Mn^{2+} in LCS at 297 K. The g_0 values as estimated from the position of the central broad line (A), without resolved hf structure, at temperatures below RT, are as follows: 2.0104 (248 K), 2.0159 (152 K), 2.0173 (82 K), and 2.0438 (3.8 K).

Spin-Hamiltonian parameters below the phase-transition temperature at 90 and 152 K

At 90 and 152 K the full 30-line Mn^{2+} spectrum could be observed for **B** along a magnetic axis that lies in the RT ac crystal plane close to the c axis, as discussed in Sec. IV. From the 30-line positions of these spectra all

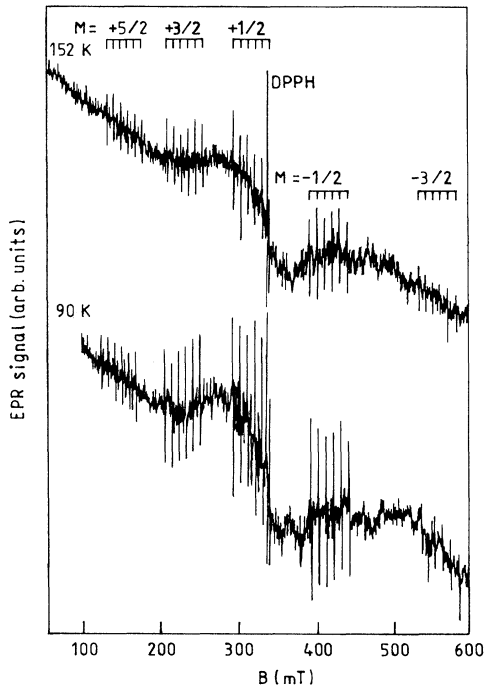

FIG. 9. Well-resolved Mn^{2+} EPR spectra at 90 and 152 K, as recorded for the orientation of the external magnetic field parallel to the magnetic x axis (close to c axis in the ac plane) in a Mn^{2+}-doped $LiCsSO_4$ crystal. The transitions M, $m \leftrightarrow M-1$, m are indicated by M, in accordance with the corresponding transitions for **B**||z.

the Mn^{2+} spin-Hamiltonian parameters can be estimated by fitting to the spin-Hamiltonian appropriate to Mn^{2+} in orthorhombic symmetry:[32]

$$\mathcal{H}=\mu_B g_{\parallel} B_z S_z+\mu_B g_{\perp}(B_x S_x+B_y S_y)+\tfrac{1}{3}b_2^0 O_2^0+\tfrac{1}{3}b_2^2 O_2^2 + \tfrac{1}{60}(b_4^0 O_4^0+b_4^2 O_4^2+b_4^4 O_4^4)+Q'[I_z^2-I(I+1)/3] + Q''(I_x^2-I_y^2)+A_{\parallel} S_z I_z+A_{\perp}(S_x I_x+S_y I_y)\ , \quad (2)$$

where μ_B is the Bohr magneton and O_l^m are the spin operators as defined by Abragam and Bleaney.[33] (It is noted that a spin Hamiltonian appropriate to orthorhombic local symmetry rather than monoclinic symmetry has been used, since experience with similar systems indicates that the local Mn^{2+} symmetry is most often orthorhombic, even in crystals with monoclinic symmetry.)

To evaluate the spin-Hamiltonian parameters, a least-squares-fitting computer procedure utilizing numerical diagonalization of the spin-Hamiltonian matrix[34,35] was employed, wherein all the 30-line positions were simultaneously fitted.

An examination of the parameter values as estimated above assuming that the magnetic axis is the z axis reveals that the absolute value of the spin-Hamiltonian parameter b_2^2 so evaluated is larger than that of b_2^0. Then, this magnetic axis is not really the magnetic z axis, for which the overall splitting of lines should be absolutely the maximum, and the magnitude of b_2^0 should be larger than that of b_2^2. This axis should then be the magnetic x axis because, these parameter values when transformed to the frame of reference where this magnetic axis is the x axis,[36,37] are indeed such that the absolute value of the transformed parameter b_2^0 is larger than that of the transformed parameter b_2^2. Finally, the values of the parameters as estimated by fitting the lines assuming that the magnetic axis is the x axis are as follows:

At 152 K

$g_{\perp}=2.005\pm0.002$, $b_2^0=2.237\pm0.001$ GHz, $b_2^2=-0.806\pm0.001$ GHz, $b_4^0=0.14\pm0.03$ GHz, $b_4^2=0.26\pm0.05$ GHz, $b_4^4=0.08\pm0.01$ GHz, $Q'=-0.012\pm0.003$ GHz, $Q''=-0.001\pm0.001$ GHz, and $A_{\parallel}=A_{\perp}=-0.267\pm0.001$ GHz.

At 90 K

$g_{\perp}=2.007\pm0.002$, $b_2^0=2.238\pm0.001$ GHz, $b_2^2=-0.844\pm0.001$ GHz, $b_4^0=0.25\pm0.03$ GHz, $b_4^2=0.71\pm0.05$ GHz, $b_4^4=0.20\pm0.01$ GHz, $Q'=-0.015\pm0.003$ GHz, $Q''=0.004\pm0.001$ GHz, $A_{\parallel}=A_{\perp}=-0.264\pm0.001$ GHz.

The value of $g_{\parallel}$ cannot be estimated as $\mathbf{B}\|\mathbf{x}$. These values represent, at each temperature, a better than 0.5% deviation of the energy of microwave quantum and the average calculated energy-level difference between levels participating in resonance. As for the absolute sign of the hf parameters, $A_{\parallel}$ and $A_{\perp}$, a negative sign has been assumed in accordance with the hyperfine-interaction data of Steudel.[38] Further, the absolute sign of the parameter b_2^0 has been determined to be positive, at both 90 and 152 K, from the spacing between the successive hyperfine lines of the highest-field sextet in the present case for $\mathbf{B}\|\mathbf{x}$, which increases with increasing magnetic-field intensity, from 8.4 to 11.2 mT (at 90 K), and over somewhat a smaller range at 152 K. To this end, higher-order perturbation corrections to the hyperfine splitting have been taken into account.[39] This yields the absolute sign of b_2^0 to be positive, while those $A_{\parallel}$, $A_{\perp}$ to be negative, the same as that determined from hyperfine-interaction data. Finally, since the relative signs of the fine-structure parameters (b_l^m) as yielded by the least-squares fitting are correct, this enables the determination of the absolute signs of *all* the parameters.

VII. THE CRITICAL EXPONENT γ

The purely transverse-acoustic mode, characterized by the elastic constant, c_{66}, drives the ferroelastic phase transition in LCS, occurring at $T_c=205$ K.[11] The temperature-dependent variation of c_{66} was found by Mróz *et al.*[11] to be $c_{66}=c|T-T_c|^{\gamma}+b$, for T above and below T_c, with the critical exponent $\gamma=1$. Assuming that the intensity of an EPR line, proportional to the first derivative of the imaginary part of the dynamic susceptibility ($d\chi''/dB$), is the order parameter in EPR, it is expected that it should exhibit a critical behavior similar to that of c_{66} near the phase-transition temperature. Examining from Fig. 8 the peak-to-peak heights (I) of line A at various temperatures, which are proportional to the respective intensities, since the width of line A is invariant with temperature, for the orientation of $\mathbf{B}$ at $+10°$ from the a axis in the ab plane, and for $\mathbf{B}$ at $-25°$ from the c axis in the ac plane, and taking into account the experimental errors, it is seen from Fig. 8 that all these plots are linear in temperature in the regions 180–200 K and 210–233 K, which lie, respectively, just below and just above the temperature region (200–210 K) over which the phase transition takes place. This implies that $I=c|T-T_c|^{\gamma}+b$, with $\gamma=1$ and is therefore in accordance with the behavior of the elastic constant c_{66}.[11]

VIII. PHASE TRANSITIONS

This section covers a discussion of those features of EPR spectra of Mn^{2+}-doped LCS, which indicate the occurrences of the various phase transitions undergone by LCS single crystals. The occurrence of a phase transition is indicated when the features of EPR spectra exhibit abrupt changes as the temperature is varied.

Reorientation of SO_4 tetrahedra in the range 233–268 K

Inspecting from Fig. 8 the dependence on temperature of (i) the peak-to-peak height (I) of line A for $\mathbf{B}$ at 10° from the a axis in the ab plane, (ii) the peak-to-peak height (I) of line A for $\mathbf{B}$ at $-25°$ from the c axis in the ac plane, (iii) the peak-to-peak height (I) of line B for $\mathbf{B}$ at $-25°$ from the c axis in the ac plane, and (iv) the width (ΔB_{pp}) of line B for $\mathbf{B}$ at $-25°$ from the c axis in the ac plane, it is seen that the plots for (i) and (ii) exhibit a

sharp drop, while those of (iii) and (iv) exhibit a general rise, as the temperature is lowered through this region. This indicates a continual reorientation of the SO_4 tetrahedra. The orientation involves a rotation about the c axis, as concluded by examining the relative orientations in Fig. 1(b) of the SO_4 tetrahedra above and below 205 K, i.e., in the paraelastic and ferroelastic phases, respectively. This orientation is a precursor to the phase transition occurring in LCS crystal at 205 K (discussed next), associated with the disorder-order transition of the SO_4 tetrahedra.

Phase transition at 205 K

It is seen from Fig. 8 that there occur sharp peaks in the height (I) versus temperature plots of the broad lines A and B for **B** at $-25°$ from the c axis in the ac plane, each centered at 205.5 K. On the other hand, the dependence of the width of line B on temperature shows the occurrence of a small peak centered at 204.5 K. Also, the slope of the height of line A versus temperature for **B** at 10° from the a axis in the ab plane changes sharply at this temperature. These indicate the occurrence of a phase transition at $T_c = 205 \pm 0.5$ K. This value is almost the same as that estimated from the splitting of NH_3^+ EPR lines in LCS: 206 K on cooling and 204 K on warming.[5,8] Techniques other than EPR yield the corresponding phase transition temperature for LCS to be 202.8 K (differential scanning calorimetry[19]) and 202 K (Raman spectroscopy,[2] Brillouin spectroscopy,[11] x-ray diffraction,[17] and specific-heat measurements[20]).

Intermediate phase

It is seen from the inset in Fig. 8 that there occur, in the temperature range 194–205 K, plateaus in the heights of the broad lines A and B for the orientation of **B** at $-25°$ from the c axis in the ac plane, and a peak in the width of line B. This temperature range is in accordance with that of the "intermediate phase" in LCS (199–206 K) observed by Yu, Chou, and Huang[5] by EPR and by Kruglik *et al.*[15] under a microscope. Specifically, Kruglik *et al.*[15] observed, under a microscope, the occurrence of twins in the form of succession of plane layers with normals parallel to the a and b axes distinguishable by their angles of extinction.

The phase transition in the 155–175 K range

It is seen in Fig. 8, that as the temperature was decreased, there occur small peaks in the heights of the broad lines A and B for the orientation of **B** at $-25°$ from the c axis in the ac plane, centered at 175 and 162 K, respectively. Also, the width of line B indicates a dip centered at 155 K. All these behaviors indicate the occurrence of a phase transition, which is spread over the 155–175 K temperature interval. This is in accordance with the occurrence of a phase transition in LCS at 160 K as deduced both from Raman spectroscopy by Morell *et al.*[2] and by the EPR of NH_3^+ and Cr^{5+} ions by Yu *et al.*[5]

The phase transition in the range 3.8–31 K.

The spectra were recorded only at 3.8 and 31 K, so it was not possible to determine the exact phase-transition temperature. At 3.8 K, there appear extra hf lines over and above those at 31 K at lower magnetic fields (Fig. 3). Also, the structure of line A at 3.8 K is different from that at 31 K. These differences can be linked to the occurrence of a possible phase transition somewhere in the range 3.8–31K, in accordance with that observed by Raman scattering,[2] deduced to be a structural phase transition of the unlocking type, occurring somewhere below 20 K, as deduced from the observed softening of optical phonons (44 cm^{-1}).

Role of impurities

The phase-transition temperatures determined presently are at slight variances with those determined by other techniques. This may be, among other factors, due to the presence of Mn^{2+} ions as impurity. The impurities play an important role in modifying the value of the phase-transition temperature, as well as spreading of the phase transition over a longer temperature interval,[28] as evidenced in Mn^{2+}-doped NH_4Br (Ref. 25) and in Cu^{2+}-doped NH_4Br (Ref. 40), where T_c was lower by 4–5 K from that determined by other measurements on undoped samples. Misra *et al.*[41] also observed a difference in the phase-transition temperature of $CaCd(CH_3COO)_4 \cdot 6H_2O$, by as much as 16 K, as determined from EPR measurements on Mn^{2+}-doped ($T_c = 146$ K) and Cu^{2+}-doped ($T_c = 130$ K) samples.

IX. CONCLUDING REMARKS

It is noted that due to small percentage of Mn^{2+} ions entering LCS crystals, the spectra were characterized by rather weak intensities of lines, especially at liquid-helium temperatures, where the high-Q Varian cavity with nitrogen gas flow was not used. The main features of the present EPR study on LCS crystals are as follows.

(i) At higher temperatures, the LCS crystals consist of twin domains.

(ii) One of the Mn^{2+} centers in LCS is effectively in the $S = \frac{1}{2}$ low-spin state in $LiCsSO_4$ at higher temperatures as revealed by the presence of the central hf sextet above 248 K.

(iii) There are detected two phase transitions undergone by LCS crystals in the temperature range 150–301 K. The so-called paraelastic-ferroelastic phase transition is determined to occur at 205 ± 0.5 K, and the incommensurate-commensurate phase transition[2] is spread over the range 155–175 K. In addition, the present data confirm the occurrence of a third phase transition of the unlocking type in LCS somewhere between 3.8 and 31 K.

(iv) The value of the critical exponent (γ) for the intensity of the central broad line as a function of temperature is consistent with that for the elastic constant c_{66}.[11]

(v) The values of the parameters g_0 and A_0 of Mn^{2+} have been determined at room temperature. At 90 and 152 K, in the monoclinic phase, where twining is absent, the values of Q', the spin-Hamiltonian parameters $g_\perp$, b_l^m, Q'', $A_\parallel$, and $A_\perp$, have been estimated.

ACKNOWLEDGMENTS

The authors are grateful to the Natural Sciences and Engineering Research Council of Canada for financial support (Grant No. OGP0004458).

*Permanent address: Department of Experimental Physics, Maria Curie-Skłodowska University, Place M. Curie-Skłodowskiej 1, 20-031 Lublin, Poland.

[1]B. C. Venkata Reddy and B. Munibhadraiah, Mater. Lett. **4**, 219 (1986).

[2]G. Morell, S. Devanarayanan, and R. S. Katiyar, J. Raman Spectrosc. **22**, 529 (1991).

[3]B. C. Venkata Reddy and B. Munibhadraiah, Ferroelectrics Lett. **5**, 57 (1985).

[4]N. R. Ivanov and A. Pietraszko, Phase Trans. **12**, 235 (1988).

[5]Jiang-Tsu Yu, Shen-Yuan Chou, and Shu-Jeu Huang, J. Phys. Chem. Solids **49**, 289 (1988).

[6]Shen-Yuan Chou and Jiang-Tsu Yu, J. Phys. Chem. Solids **51**, 993 (1990).

[7]Jiang-Tsu Yu, J. Phys. C **21**, 759 (1988).

[8]Shu-Jeu Huang and Jiang-Tsu Yu, Solid State Commun. **63**, 745 (1987).

[9]P. C. Morais, G. M. Ribeiro, and A. S. Chaves, Solid State Commun. **52**, 291 (1984).

[10]K. S. Aleksandrov, M. P. Zaitseva, L. A. Shabanova, and O. V. Shimanskaya, Fiz. Tverd. Tela (Leningrad) **23**, 2440 (1981) [Sov. Phys. Solid State **23**, 1426 (1981)].

[11]B. Mróz, H. Kiefte, M. J. Clouter, and J. A. Tuszyński, Phys. Rev. B **36**, 3745 (1987).

[12]B. Mróz, J. A. Tuszyński, H. Kiefte, and M. J. Clouter, Ferroelectrics **107**, 155 (1990).

[13]F. Hołuj, Ferroelectrics **65**, 55 (1985).

[14]F. Hołuj, Ferroelectrics **67**, 103 (1986).

[15]A. I. Kruglik, M. A. Simonov, E. P. Zhelezin, and N. V. Belov, Dokl. Akad. Nauk SSSR **247**, 1384 (1979) [Sov. Phys. Dokl. **24**, 596 (1979)].

[16]T. Asahi and K. Hasebe, J. Phys. Soc. Jpn. **57**, 4184 (1988).

[17]A. Pietraszko, P. E. Tomaszewski, and K. Łukaszewicz, Phase Trans. **2**, 141 (1981).

[18]W. Bronowska and J. Dziedzic, Ferroelectrics **79**, 455 (1988).

[19]T. Hidaka, Phys. Rev. B **45**, 440 (1992).

[20]K. S. Aleksandrov, L. I. Zherebtsova, I. M. Iskornev, A. I. Kruglik, O. V. Rozanov, and I. N. Flerov, Fiz. Tverd. Tela (Leningrad) **22**, 3673 (1980) [Sov. Phys. Solid State **22**, 2150 (1980)].

[21]B. Raghunatha Chary, M. N. Shashikala, and H. L. Bhat, Current Sci. **55**, 1021 (1986).

[22]T. I. Chekmasova, I. S. Kabanov, and V. I. Yuzvak, Phys. Status Solidi A **44**, K155 (1977).

[23]S. Fujimoto, N. Yasuda, and H. Hibino, J. Phys. D **18**, 1871 (1985).

[24]S. V. J. Lakshman and A. Sundar Jacob, Phys. Lett. **101** A, 109 (1984).

[25]P. Chand and G. C. Upreti, J. Phys. Soc. Jpn. **54**, 2311 (1985).

[26]Th. Frey, M. Maier, J. Schneider, and M. Gehrke, J. Phys. C **21**, 5539 (1988).

[27]M. D. Sastry, Ph.D. thesis, I. I. T., Kanpur, India, 1967 (unpublished).

[28]D. Shaltiel, A. Grayevsky, V. Zevin, and G. Grüner, Phys. Rev. B **38**, 10 075 (1988).

[29]Jiang-Tsu Yu, Ying-Sheng Huang, and Shoei-Sheng Lin, J. Phys. Condens. Matter **2**, 5587 (1990).

[30]S. Ohnishi and S. Sugano, J. Phys. C **14**, 39 (1981).

[31]N. M. Atherton, *Electron Spin Resonance* (Wiley, New York, 1973).

[32]V. M. Vinokurov, M. M. Zaripov, and V. G. Stepanov, Fiz. Tverd. Tela (Leningrad) **6**, 1130 (1964) [Sov. Phys. Solid State **6**, 870 (1964)].

[33]A. Abragam and B. Bleaney, *Electron Paramagnetic Resonance of Transition Ions* (Clarendon, Oxford, 1970).

[34]S. K. Misra, J. Magn. Reson. **23**, 403 (1976).

[35]S. K. Misra, Physica B **121**, 193 (1983).

[36]S. K. Misra, Magn. Reson. Rev. **10**, 285 (1986).

[37]D. A. Jones, J. M. Baker, and D. F. D. Pope, Proc. Phys. Soc. (London) **74**, 249 (1959).

[38]A. Steudel, *Hyperfine Interactions* (Academic, New York, 1976), p. 182.

[39]B. Bleaney and D. J. E. Ingram, Proc. R. Soc. Ser. A **205**, 336 (1951).

[40]N. J. Trappeniers, F. S. Stibbe, and J. L. Rao, J. Phys. Chem. Solids **42**, 616 (1981).

[41]S. K. Misra, M. Kahrizi, and S. Z. Korczak, Physica B **182**, 186 (1992).